# Tensile response of screw piles with varying installation approaches in layered sand

Pelluru Venkata Pavan Kumar, Wei Wang*, Michael John Brown, Shantanu Patra, Sumanta Haldar, Yaseen Umar, Sharif, Jonathan Adam Knappett

Mr. Pelluru Venkata Pavan Kumar,
PhD research Scholar, School of Infrastructure, IIT Bhubaneswar 752050, India.
ORCID: 0000-0003-0411-7698
Email: pvk11@iitbbs.ac.in

*Corresponding author
*Mr Wei Wang, BSc, MSc
PhD student, School of Science and Engineering, University of Dundee, Fulton Building, Dundee, DD1 4HN, UK
ORCID: 0000-0002-3838-2142
Email: 2422030@dundee.ac.uk

Prof Michael John Brown, BEng (Hons), PhD, GMICE
Professor of Geotechnical Engineering, School of Science and Engineering, University of Dundee, Fulton Building, Dundee, DD1 4HN, UK
ORCID: 0000-0001-6770-4836
Email: m.j.z.brown@dundee.ac.uk

Prof Shantanu Patra
Associate Professor, Department of Civil Engineering, School of Infrastructure, IIT Bhubaneswar 752050, India.
ORCID: 0000-0001-8827-8194
Email: shantanupatra@iitbs.ac.in

Prof Sumanta Haldar
Professor, Department of Civil Engineering, School of Infrastructure, IIT Bhubaneswar 752050, India.
ORCID: 0000-0002-8575-8317
Email: sumanta@iitbbs.ac.in

Dr Yaseen Umar Sharif, MEng (Hons), GMICE
Research Associate, School of Science and Engineering, University of Dundee, Fulton Building, Dundee, DD1 4HN, UK
ORCID: 0000-0002-3620-7500
Email: y.sharif@dundee.ac.uk

Prof Jonathan Adam Knappett, MA MEng PhD CEng MICE
Professor of Civil Engineering, School of Science and Engineering, University of Dundee, Fulton Building, Dundee, DD1 4HN, UK
ORCID: 0000-0003-1936-881X
Email: J.A.Knappett@dundee.ac.uk

Word count: 5798

Figure numbers: 16

Table numbers: 7



This is the accepted manuscript of: Kumar, PVP, Wang, W, Brown, M, Patra, S, Haldar, S, Sharif, Y & Knappett, J 2025, 'Tensile response of screw piles with varying installation approaches in layered sand', Proceedings of the Institution of Civil Engineers: Geotechnical Engineering. https://doi.org/10.1680/jgeen.24.00385

## Abstract

Single or multiple helix screw piles are being considered as fast and economical foundation systems for onshore renewable energy units. These foundations may encounter distinct soil layering and need to perform under a variety of load cases. For this application, installation and monotonic tensile load response of multiple helix screw piles in uniform and layered sands was investigated by centrifuge modelling. Standard pitch-matched and pile self-weight approaches to installation were considered. The latter is advantageous as it requires no additional vertical force during installation (minimising plant requirements) alongside improved tensile capacity and reduced installation torque. Tensile capacity could also be increased by the inclusion of additional helices but soil properties and layering arrangement must be considered or tensile capacity may be reduced. Performance of existing tensile capacity design methods was investigated and compared with the tests results. A cylindrical shearing mechanism appears appropriate for capacity prediction in the majority of layering arrangements explored. Where individual plate-bearing mechanisms dominate, a modification to an existing approach reasonably predicted tensile capacity for shallow mechanisms, while further work is required to develop reliable prediction methods for deep mechanism behaviour in layered soils.



**Keywords:** Foundations, Piles & Piling, Centrifuge Modelling, Sands, Screw piles, Helical anchors


## 1 Introduction

Screw piles are generally comprised of single or multiple helices welded to a central shaft (Perko 2009). This type of pile has been widely used due to its ease of installation and high tensile capacity compared to conventional straight-shafted piles with the same shaft diameter (Al-Baghdadi 2018). Recently, screw piles have received increasing attention as efficient foundation and anchoring solutions for the renewable energy sector e.g. solar (Feng *et al.* 2020) and onshore and offshore wind, where tensile capacity is a key control on design (Cerato and Victor 2009; Cerfontaine *et al.* 2023b; Davidson *et al.* 2022; Kumar *et al.* 2023; Spagnoli and Tsuha 2020).

To install a screw pile, the required installation vertical force (also termed crowd or thrust force) and torque typically increases with soil strength, pile shaft and helix diameters and number of helices. Control of installation is also an influencing factor. To minimise soil state changes induced by installation, current standards e.g. British Standards Institution (2015) suggest a pitch-matched (PM) approach where advancement ratio (AR) is controlled, being AR =1.0 (Eq. 1) with ± 15% tolerance (Bradshaw *et al.* 2019):

$$AR = \frac{\Delta z}{p_h} \quad (1)$$

where $\Delta z$ is pile vertical penetration in a single rotation and $p_h$ is the helix geometric pitch.

This displacement-controlled methodology has been widely adopted for scaled laboratory tests (Li *et al.* 2022; Schiavon *et al.* 2017) but has been shown to be impractical in the field as prohibitively high installation vertical force can be required (Davidson *et al.* 2022). It has been proposed that screw piles may be over-flighted (AR < 1.0) to reduce installation force and improve tensile performance at the expense of reduced compressive capacity (Bittar *et al.* 2024; Cerfontaine *et al.* 2023a; Sharif *et al.* 2021a; Wang *et al.* 2025a). It is also possible to install screw piles in a force-controlled manner e.g. under their own self-weight. Bradshaw *et al.* (2019) installed screw piles by applying torque and dead weight on the pile head and found that AR tended to stabilise at 0.3 < AR < 0.8. Ullah *et al.* (2023) showed in clays that screw piles can be installed to a target depth by rotating the pile with only pile self-weight. This self-weight (SW) installation may allow piling where available reaction force is limited, e.g. lightweight installation equipment. However, effects of a self-weight installation approach on pile loading response need to be further investigated and are considered as part of this paper.

Previous screw pile studies have focussed on uniform soils, although a limited number of investigations of buried anchor plates have considered layered soils. Bouazza and Finlay (1990) conducted 1g tests of shallow plate anchors (embedment depth/plate width, $B/D_h < 5$) in sand and found that overlying looser layers decreased tensile capacity. Srinivasan *et al.* (2019) attempted to consider layering by averaging soil unit weight and friction angle above the plate, but previous study have shown that a plate (shallow, $B/D_h < 7$) in loose sand with overlying dense soil exhibited lower tensile capacity compared to loose over dense soil setups (Bhattacharya and Kumar 2016; Sakai and Tanaka 2007), apparently indicating that soil closer to the anchor contributes more to the capacity and the layering effect cannot be considered by simply averaging soil properties.

In this study centrifuge tests were conducted to investigate installation and tensile performance of screw piles in dry layered sand soil beds. Piles with different numbers of helices/spacing were considered to inform future pile design optimisation strategies. Pitch-matched, over-flighted displacement-controlled and self-weight installation approaches were considered. Existing design methods for tensile capacity prediction were considered and improvements suggested to account for soil layering effects.

## 2 Centrifuge modelling methodology

### *2.1 Experiment setup*

Tests were undertaken on the University of Dundee's 3 m radius beam centrifuge at 30g at a scale of 1:30. Installation and subsequent loading were conducted in a single centrifuge flight. This was achieved using a bespoke two-axis actuator controlling the rotational and vertical displacement of the model piles. Vertical force and torque were continuously measured by a combined axial force – torque load cell (F310-Z, Novatech Measurements Ltd), rigidly connected to the pile head, with a range of $\pm$30 Nm (torque) and $\pm$20 kN (force). Note that the piles were not instrumented and thus only total vertical force and torque on the pile heads were measured and contribution of each pile component (each helix and pile shaft and base) was not directly separately assessed. Although without a direct assessment in this study, the contribution of the shaft friction has been reported to be small (typically < 15%) regarding to both installation and in-service and loading is predominately carried by the helix during a monotonic tensile test (Schiavon 2016; Sharif *et al.* 2021b). Vertical displacement was measured by a WPS-500-MK30 draw-wire sensor. More details of the actuation systems can be found in (Davidson *et al.* 2018; Wang *et al.* 2023).

### *2.2 Soil preparation*

All dry soil beds were 434 mm deep and were created by air pluviating HST95 sand into a 500 mm × 800 mm × 550 mm strong box. HST95 sand is a fine-grained quartz sand that has been extensively used and characterised at the University of Dundee (Al-Defae *et al.* 2013; Lauder 2010). Properties of HST95 sand are given in Table 1. All subsequent properties are given at prototype scale, unless otherwise stated.

Four soil bed configurations were considered (Figure 1). The benchmark case was uniform and dense (UD, relatively density $D_r$= 75%). Soil bed DOL (dense-over-loose, Figure 1a) had a 3 m thick dense layer ($D_r$ = 75%) overlying loose sand ($D_r$ = 30%). Soil bed LOD (loose-over-dense, Figure 1b) was the reverse of DOL. A third "sandwich" case (DLD Figure 1c) consisted of a 1.5 m loose layer sandwiched between a 1.5m dense layer (above) and dense soil below. The pile geometries investigated are indicated schematically in Figure 1. Formation of layers was checked in-flight by means of a miniature CPT (Figure 2) and density pots after testing.

### *2.3 Pile models*

Model piles with two and three helices (as shown in Figure 3) were created from 316L stainless steel using 3D metal printing. All dimensions discussed in this section are at prototype scale. The piles had asymmetric 45° cut-off tips, with a 600 mm diameter ($D_{h,b}$) helix immediately above with a geometric pitch of 309 mm. This bottom helix was relatively small

($D_{h,b}$ = twice shaft diameter $= 2D_s$) to minimise installation requirements but was included to aid installation. The top helix was located at 750 mm below the soil surface (5.25 m above the pile tip) and had a larger diameter $D_{h,t}$ = 1200 mm for improved near surface lateral loading response (not considered in this study; (Al-Baghdadi *et al.* 2015). The piles were designed such that the upper helix was in the upper soil layer and the lower helix was in the lower layer (Figure 1).

Based on helix embedment depth, different failure mechanisms can occur for the dual-helix (2H) pile (Figure 4). Assumptions about the likely failure mechanisms were initially made as part of pile design. A shallow mechanism refers to a failure that develops from a helix up to the ground surface as a truncated cone with an inclined angle equal to soil peak dilation angle (Ghaly *et al.* 1991; Giampa *et al.* 2017). In contrast, a deep mechanism involves localised flow-around failure. However, for calculation simplification, the deep mechanism shape is often assumed as a truncated cone with limited height where the height tends to increase with soil relative density (Ghaly *et al.* 1991). The embedment depth ratio (depth to helix diameter, $H/D_h$) at mechanism transition is typically related to soil relative density (peak friction and dilatancy angle). In this study, the transition would be expected at $H/D_h$ = 6.0 for loose sand and $H/D_h$ = 10.0 for dense sand (Al Hakeem and Aubeny 2019; Ghaly *et al.* 1991; Mitsch and Clemence 1985). Therefore, for the 2H pile in bed DOL, a deep mechanism was assumed for the bottom helix (embedment ratio $H_b/D_{h,b}$ = 9.2) while for the top helix ($H_t/D_{h,t}$ = 0.6) a shallow failure mechanism was assumed (Figure 4b). As shown in Figure 4b, the deep mechanism should be a flow around (solid line); however, for comparison the shape of deep failure mechanisms can be also assumed as a truncated cone with restricted height as proposed by per Ghaly *et al.* (1991) (dashed line). In all other soil beds, the failure mechanism for both the bottom and top helices was assumed to be shallow, but the latter may be subsumed by the former and therefore the top helix may not provide significant additional tensile capacity in these cases (Figure 4a, c and d).

The three-helix pile (3H) was similar to 2H with the inclusion of a second large-diameter middle helix located 2.4 m ($S_{h,tm}$ = $2D_{h,m}$ or $2D_{h,t}$) below the top helix (2.85 m above pile tip) resulting in the spacing between the bottom and middle helices ($S_{h,mb}$) being three times the average diameter ($0.5D_{h,m}$+$0.5D_{h,b}$). When helix spacing $S_h/D_h$ is small i.e. typically less than 3.0 (Knappett *et al.* 2014; Lutenegger 2011), soil trapped between helices is mobilised forming a cylindrical soil-soil shear surface. Therefore, for the 3H pile the cylindrical shearing mechanism was assumed between the helices leaving a shallow truncated cone failure above the top helix in all soil beds (Figure 4). For the 3H pile the middle helix was designed to be just below the lower layer boundary (LB) in all three layering cases considered (0.15 m or $0.13D_{h,m}$; Figure 1). Both piles had solid pile shafts to avoid structural damage during testing and create a consistent plugged pile response.

The weights of the 2H and 3H piles at the target g-level (30g) were 0.0435 kN and 0.0493 kN at model scale, corresponding to 39.2 kN and 44.4 kN at prototype scale, respectively. These weights are much smaller than the pile tensile capacities, which reach up to several hundred kN (see testing results presented in Section 3).

### *2.4 Test procedures*

The box dimensions allowed two piles to be installed and tested in a single box (Figure 5). Each pile location was at least $12D_{h,b}$ from box horizontal boundaries or the other pile. The pile tip at the end of installation was $12D_{h,b}$ above the box bottom boundary. This exceeds previous guidance for push-in piles i.e. $10D_s$ (shaft diameter) in the radial (Bolton *et al.* 1999) and $5D_s$ in the vertical direction (Yang 2006) to avoid boundary effects during installation.

All pile installations were conducted at a constant rotation rate (3 revs/min). For displacement-controlled installations, a constant vertical velocity was chosen consistent with the desired AR. For force-controlled (SW) installation, a user configurable PID (Proportional Integral Differential) controller was utilised with the vertical drive axis. The value of the target input force was equal to the pile weight (at 30g) to simulate a rotation-only self-weight installation and remained constant throughout SW installation. As the initial force signal cannot be zero for force-controlled installation, SW cases were initially displacement-controlled to an initial depth before switching to force-controlled mode. This initial depth was $1.0D_{h,b}$, except in the case of the 2H pile in the LOD bed where a PID controller fault occurred when switching from displacement-controlled to force-controlled mode and the initial installation depth was $2.0D_{h,b}$. This fault was unlikely to make a significant difference to subsequent tensile response as it occurred at limited depth where the soil was expected to make minimal contribution to tensile capacity.

To determine tensile capacities (peak loading), the piles were uplifted to a maximum displacement of 300 mm ($0.5D_{h,b}$) at a constant velocity of 1 mm/s (model scale). Table 2 summaries the test configurations discussed herein. The test identification (ID) nomenclature was given as 'pile ID_ soil bed ID_ installation mode' e.g. 2H_UD_AR1 reflects a dual-helix pile installed in uniform density sand at AR=1.

## 3 Results and discussions

### *3.1 Effects of soil profile and pile design under pitch-matched installation*

#### *3.1.1 Installation response*

Figure 6 and Figure 7 show the vertical force and torque developed, respectively, when installing the piles at AR = 1.0 (pitch matched) in different ground conditions. Both increase with depth more rapidly when the pile tip and bottom helix are in a denser layer. A sharp increase in force and torque growth rate appears at a depth of z = -5.25 m for pile 2H in DOL

and UD cases when the top helix entered the upper dense layer. This was absent for pile 3H, due to the passage of the large mid helix disturbing the surrounding soil. Soil disturbance induced by helix passage and its effects on the response of following helices in uniform ground conditions have been reported in previous studies (Tsuha *et al.* 2012).

### *3.1.2 Tensile response*

Figure 8(a) shows the load – displacement response during tensile tests for all AR = 1.0 cases. The maximum tensile force (tensile capacity, $Q_t$) occurs at uplift displacements ranging from 0.07 m to 0.11 m ($0.12D_{h,b}$ to $0.18D_{h,b}$ or $0.06D_{h,t}$ to $0.09D_{h,t}$). Figure 8(b) suggests that the consequence of inclusion of the mid helix depends on the soil bed profiles. The significantly enhanced tensile capacity induced by the additional middle helix for the 3H pile in the DOL case is consistent with the differences in assumed failure mechanism (Figure 4b), where the cylindrical shearing mechanism linking the three helices results in a significantly larger shear area compared to localised mechanisms around the individual helices of the 2H pile. However, for the other soil profiles the inclusion of the mid helix does not improve (LOD) and can even reduce tensile capacity (UD and DLD) as shown in Figure 8(b). This is consistent with disturbance induced by the passage of the middle helix under PM conditions – in the LOD case, disturbance (to critical state) does not alter the soil state significantly as it is already loose, whereas significant softening would be expected from dense to critical state conditions (UD and DLD). For the scenarios explored herein, it is possible to increase tensile capacity of a predominantly 'deep' mechanism screw pile by inclusion of additional helices e.g. near to an overlying stiffer/denser soil layer (Figure 4b), while for 'shallow' mechanism screw piles additional helices tend to intensify soil disturbance and reduced tensile capacity (Figure 4a, c and d). Another key practical implication (Figure 8) is that where it is desirable to have a near-surface helix for lateral capacity, addition of an intermediate helix and the disturbance it induces can be harnessed to significantly reduce the variability of the capacity of a standardised pile design for an application where ground conditions across a site may be variable.

## ***3.2 Effect of installation approach***

### *3.2.1 Installation response*

Apart from standard pitch-matched installation (AR = 1.0), self-weight installation (SW) was also conducted for both 2H and 3H piles in DOL and LOD soil beds. All SW piles were successfully installed to the target depth of 6 m under the self-weight conditions. Figure 9 shows the measured AR values for all SW installations. Once SW installation starts, AR reduces quickly from 1.0, which is consistent with previous experimental and numerical observations (Sharif 2024; Ullah *et al.* 2023). The case of 2H LOD shows higher AR values than the other three cases at $z$ > -2 m, due to the additional initial penetration at AR =1.0. In the other cases, no remarkable difference is seen down to the depth of $z$ = -1.5 m. Overall, the measured AR values throughout installation varied from 0.35 to 1.0 but tends to 0.6 to 0.8 towards the end of installation

and below the layer boundary. The AR values in Figure 9 remain broadly stable towards the end of installation suggesting that the piles could have penetrated further using the self-weight mode (significant reduction in AR, i.e. pile only rotating without vertical penetration, would suggest the onset of refusal).

Similar to PM installation, Figure 9 also suggests that AR values during SW installation are affected by soil bed profiles and helix number. At -1.5 m > $z$ > -3.0 m (the bottom helix is in the first layer and the mid-height helix of 3H has not penetrated the ground), AR values for DOL are lower (greater over-flighting) than those for LOD for both 2H and 3H consistent with generating increased tensile pull-in force to overcome the higher penetration resistance in the upper denser layer (Figure 10a; (Cerfontaine *et al.* 2021). When the bottom helix encounters the lower layer ($z$ < -3m), penetration resistance reduces for piles in DOL cases resulting in higher AR values compared to piles in LOD cases. When comparing 2H and 3H piles (in either layering case), the 3H pile shows higher AR values after the middle helix enters the soil because the over-flighted middle helix provides additional tensile force to pull the pile into ground (Figure 10b).

Figure 11 shows force and torque measured during SW installation of the 3H pile in the DOL case, with comparison to those during displacement-controlled installations (conducted at AR = 1.0 and 0.35). AR = 0.35 represented the lower bound of AR values observed above the layer boundary during SW installation (Figure 9). The constant zero vertical force for self-weight installation observed in Figure 11(a) indicates successful servo control. Installation at AR = 0.35 led to increasing tensile force during installation, i.e. the pile pulled itself into ground and the actuator needed to resist the tensile force instead of applying compressive force. This was due to increased downward force on the helix upper surface ($F_{h,u}$, Figure 11a) and decreased upwards force on the helix lower surface ($F_{h,l}$) resulting from soil being extracted up through the helix (Sharif *et al.* 2021a). Similarly, the torque required for SW installation lies between that required for installation at AR =1.0 and 0.35. The increase of $F_{h,u}$ (and resulting in increase of torque on the helix upper surface, $T_{h,u}$, Figure 11b) is less than the decrease of $F_{h,l}$ (and $T_{h,l}$) resulting in a net decrease of total torque on the helix (Cerfontaine *et al.* 2021).

*3.2.2 Tensile response*

Figure 12(a) shows that, for the 3H pile, DOL case as an example, SW installation leads to a loading capacity/stiffness between that observed for installation at AR = 1.0 and 0.35, and therefore enhanced compared to conventional PM installation at AR = 1.0. The value of AR = 0.35 is chosen here because it was the lower limit of AR during SW installation (Figure 9).This AR was included to highlight that the installation torque (Figure 11) and in-service performance (Figure 12a) of a pile installed under self-weight fall between those of the pile installed at the lower and upper bounds of AR values

involved in self-weight installation. Therefore, installation at AR = 0.35 was only conducted in a single case i.e. 3H in DOL soil bed.

Figure 12(b) shows that this was true for all of the studied pile geometries and soil bed profiles. However, it is noted that, for installation at AR = 1.0 in LOD soil bed, the 3H pile exhibits a slightly increased tensile capacity over the 2H pile. This is in contrast with SW installation in the LOD soil bed, where tensile capacity of 3H is slightly lower than the 2H pile. This is likely to be due to over-flighting of the middle helix which removes soil between the bottom and middle helix resulting in reduced soil stress on the cylindrical shearing mechanism formed between the two helices (Wang *et al*. 2025b). Therefore, design of number or spacing of helices needs careful consideration when screw piles are installed using over-flighting (or self-weight) approaches particularly where capacity is dependent on helix interaction. As with PM installation (Figure 8), where it is desirable to have a near-surface helix for lateral capacity, addition of an intermediate helix and the disturbance it induces appears to significantly reduce the variability of the capacity of a standardised pile design for an application where ground conditions across a site may be variable.

## 4 Tensile capacity calculation for screw piles in layered soil beds

Although the tensile capacity of a screw pile may be estimated in unform soil conditions for simple pile geometries, this is not a straightforward task for multiple soil layers and multi-helix piles with different competing failure mechanisms. As a starting point, the applicability of existing estimation methods was assessed. The 2H and 3H piles were considered separately because no universal method is applicable for both individual bearing (2H) and cylindrical shearing (3H) mechanisms (Figure 4).

### *4.1 Individual bearing resistance (2H pile)*

As shown in Figure 4, an individual truncated cone failure mechanism is expected for the double helix (2H) pile, and each helix can be assumed to operate as an individual anchor plate due to the inter-helix spacing. In addition, except in the DOL case (deep mechanism), the bottom helix in the remainder of soil beds is assumed to act via a shallow mechanism due to the large inter-helix spacing ($S_h/D_{h,b}$ = 8, or $S_h/D_{h,avg}$ = 5.3 based on the average helix diameter).

#### *4.1.1 Evaluation of Giampa et al. (2017) analytical method*

For shallow failure, Giampa *et al.* (2017) assumed a truncated cone failure mechanism where the inclination angle of the shear surface is equal to soil dilation angle, $\psi_p$ and proposed a non-associated flow analytical model for tensile capacity of

circular plate anchors. The individual bearing tensile capacity $Q_{t,ind}$ is the sum of soil weight within the wedge $W_c$ (Eq. 3) plus shear resistance between the wedge and the surrounding soil, $F_s$ (Eq. 4), which is equal to ultimate shear stress, $\tau$ (Eq. 5-6) integrated along the failure mechanism surface:

$$Q_{t,ind} = W_c + F_s \tag{2}$$

$$W_c = \frac{\pi}{3}\gamma H\left[\left(\frac{D_h}{2} + Htan\psi_p\right)^2 + \frac{D_h}{2}\left(D_h + Htan\psi_p\right)\right] \tag{3}$$

$$F_s = \frac{\pi}{2}H^2 C\left(D_h + \frac{2}{3}Htan\psi_p\right) \tag{4}$$

$$C = cos\left(\varphi_p - \psi_p\right)\left(tan\varphi_p - \psi_p\right)\gamma \tag{5}$$

$$\tau = Cz \tag{6}$$

where $z$ is the depth of a point of consideration in the soil, $C$ is a soil shear strength factor, $H$ is the plate or helix embedment depth, $D_h$ is the plate or helix diameter, $\varphi_p$ is the soil peak friction angle and $\psi_p$ is the soil peak dilation angle. Although installation effects are not incorporated, this method was shown to give reasonable predictions for shallow single-helix screw piles installed at AR = 1.0 in previous studies e.g. Cerfontaine *et al.* (2023a).

The Giampa *et al.* (2017) method has here been modified to apply to layered soil beds as illustrated in Figure 13. Where the pile situation displays a deep mechanism, e.g. DOL (Figure 13b and c), it has been assumed for comparison purposes that a small, localised truncated cone will form as proposed by Ghaly *et al.* (1991). In each soil layer the failure mechanism remains a truncated cone inclined at the soil dilation angle of the current layer, and the shear surface is continuous at layer boundaries. In layered soil beds, $W_c$ and $F_s$ can be calculated from Eq.7-9.

$$W_c = \sum_{i=1}^{n}\frac{\pi}{3}\gamma l_i\left[\left(\frac{B_i}{2} + l_i tan\psi_{pi}\right)^2 + \frac{B_i}{2}\left(B_i + l_i tan\psi_{pi}\right)\right] \tag{7}$$

$$F_{s,i} = \begin{cases} \pi C_i\left(\frac{B_1}{2}{H_1}^2 - \frac{B_1}{2}{H_{i+1}}^2 + \frac{tan\psi_{pi}}{3}{H_1}^3 - H_1{H_{i+1}}^2 tan\psi_{pi} + \frac{2tan\psi_{pi}}{3}{H_{i+1}}^3\right) & (i = 1) \\ \pi C_i\left(\frac{B_1}{2}{H_i}^2 - \frac{B_1}{2}{H_{i+1}}^2 + H_1{H_i}^2 tan\psi_{pi} - H_1{H_{i+1}}^2 tan\psi_{pi} - \frac{2tan\psi_{pi}}{3}{H_i}^3 + \frac{2tan\psi_{pi}}{3}{H_{i+1}}^3\right) & (i > 1) \end{cases} \tag{8}$$

$$F_s = \sum_{i=1}^{n} F_{s,i} \quad (9)$$

where $B_i$ is the diameter of the bottom end of the $i^{th}$ truncated cone failure mechanism (where $B_1 = D_h$), and $l_i$ is the height of the $i^{th}$ truncated cone failure mechanism, $H_i$ is the depth of helix *i* or depth of boundary soil layers (or failure mechanism), and $C_i$ and $\psi_{pi}$ are the strength factor and peak dilation angle of the $i^{th}$ soil layer, respectively.

As expected, the calculated capacities based on the top helix $Q_{t,gia,ht}$ are minimal (Table 3), indicating that while a near-surface upper helix may be beneficial for lateral resistance, it is the (smaller) bottom helix that controls the uplift resistance. Except for the (deep) DOL case, the uplift predictions are reasonable for the other cases under PM conditions, although with slight overestimations indicating potential soil disturbance induced during installation as shown in Figure 14(a). For the DOL case, the effect of varying the mechanism geometry was explored assuming increasing height of the truncated cone equivalent mechanism. The length of the lower truncated cone $l_1$ (lower soil layer) was varied up to the point where interaction would occur with the layer above (e.g. $l_1$ = 2.5 m) after this point the truncated mechanism was allowed to move into the soil layer above and the height of $l_2$ varied (Figure 13c). Figure 14(b) would appear to suggest that the capacity in the DOL case under PM installation is governed by a mechanism that is controlled by the lower loose sand layer with all of this layer above the lower helix being mobilised. SW installation (DOL) mobilises greater capacity which appears to include some soil in the upper dense layer, based on the limited height truncated cone approximation used herein.

For further verification of the proposed modifications, the approach was applied to an external dataset reported by Bouazza and Finlay (1990) who conducted 1g model tests of a plate anchor in dense sand underlying looser layers (LOD). The model tests involved a circular wished-in-place anchor plate with diameter $D_h$ = 37.5 mm, embedded in Leighton Buzzard sand at $H/D_h$ = 2 to 5 (shallow mechanism anticipated). Unfortunately not all of the necessary soil parameters (for 1g tests where effective stress is low as < 5 kPa) were available from the original study and thus peak friction angle $\varphi_p$ and dilation angle $\psi_p$ were back-calculated from the Bouazza and Finlay (1990) data for tests in uniform sand. Figure 15 shows that the predictions reasonably match the Bouazza and Finlay (1990) test results in layered sand.

#### *4.1.2 Evaluation of empirical methods for deep failure (DOL)*

Although the modified Giampa *et al.* (2017) method works for shallow failures, application to a deep mechanism requires determination of the failure mechanism height (e.g. DOL in this study; Figure 14b). Alternatively, Stewart (1985) suggested, for a deep plate anchor mechanism in loose/soft soil, that the overlying layers can be simply regarded as a surcharge with

unit weight that reflects the density of the overlying soil layer. To calculate tensile capacity of a deep failure mechanism, a dimensionless break-out factor $N_r$ is typically used as per Eq. 10 (Meyerhof and Adams 1968):

$$Q_t = N_r \sigma_z' \pi {D_h}^2/4 \quad (10)$$

where $\sigma_z'$ is soil vertical stress at the depth of the helical plate and $N_r$ increases with depth for shallow failure and remains constant for a deep mechanism. Several empirical methods have been proposed to estimate $N_r$ related to soil properties (Al Hakeem and Aubeny 2019) although these do not consider soil layer effects. $N_r$ was derived for the 2H pile in DOL soil from the original empirical models (for both helical plates and plate anchors), where parameters consistent with $D_r$ = 30% were adopted and for the overlying dense layer an increase of soil unit weight in Eq. 10 was adopted as per Stewart (1985). The resulting tensile capacities are shown in Table 4. The variability in the proposed $N_r$ values from the different previous studies is clear and results in significant variability of the uplift capacity prediction. The general trend of overprediction may be as a result of limitations in the experimental methodologies i.e. with no installation effects modelled (except in Mitsch and Clemence (1985) and with greater dilation in 1g physical model tests due to low confining stresses. Values of $N_r$ were also back-calculated based on the measured $Q_t$ in DOL (Table 4) and they are much lower than previous empirical model predictions.

#### *4.1.3 Evaluation of a CPT-based method (UWASP-22)*

Performance of a CPT-based tensile capacity prediction method (UWASP-22; (Bittar *et al.* 2024)) was also investigated to evaluate its performance in the layered soils considered herein:

$$Q_{hi,uwa} = \alpha_h q_{c0} \pi {D_{hi}}^2/4 \quad (11)$$

$$Q_{s,uwa} = \alpha_s q_{cs} \pi D_s L_{shaft} \quad (12)$$

$$Q_{t,uwa} = Q_{s,uwa} + \sum Q_{hi,uwa} \quad (13)$$

where $\alpha_h$ (=0.15) and $\alpha_s$ (=0.0043) are empirical factors for helix resistance and shaft resistance, respectively, $Q_{hi}$ is the tensile capacity of the $i^{th}$ helix, $D_{hi}$ is the diameter of the $i^{th}$ helix, $q_{c0}$ is the average value of cone resistance $q_c$ within $1D_{hi}$ above and below the location of the $i^{th}$ helix, $L_{shaft}$ is the shaft length, $D_s$ is the pile shaft diameter and $q_{cs}$ is the average $q_c$ from ground surface to a depth of $H_i$.

Bittar *et al.* (2024) stated that this method was only applicable for individual bearing mechanisms or widely spaced helices ($S_h/D_h$ > 3) and relatively deep helices ($H/D_h$ > 5), consistent with the 2H piles. Therefore, the embedment ratio of the top

helix ($H_T/D_{h,t}$ = 0.6) is not suited to this method. However, the contribution of the top helix is limited as indicated in Table 3 and therefore it is ignored herein. In addition, the database used to develop this method shows significantly scattered installation approaches with AR values ranging from 0.5 to 2.0.

The calculated tensile capacity using UWASP-22 is shown in Table 5 along with the contribution from the various elements of the pile. Figure 16 shows that the UWASP-22 significantly underestimates capacities for the UD and DLD cases, although predictions for DOL and LOD fall between the measured capacities at AR = 1.0 and self-weight installation conditions which may suggest some merit of this method.

In addition, UWASP-22 gives similar predictions across different layering conditions (UD, LOD and DLD) which are not consistent with experimental results and suggest a lack of sensitivity to the upper soil layers. This is due to the helix resistance calculation only considering $q_c$ values near to the helix depth and soil property variation with depth only being incorporated within the shaft component. Therefore, the form of UWASP-22 method may be more suited to deep helical plates where failure is a localised flow around mechanism e.g. DOL in this study where the prediction falls between measured capacity post installation at AR = 1.0 under self-weight. For shallow helical plates, a potentially more suitable form of $q_{c0}$ in Eq. 11 may be the average cone resistance above the helix depth over a greater zone of influence or number of equivalent helix diameters depending on the prevailing mechanism.

### *4.2 Cylindrical shearing resistance (3H pile)*

For the 3H pile the top helix is assumed to create (Figure 4): (i) a shallow individual bearing mechanism above the top helix, with capacity calculated following Section 4.1 (although the magnitudes are minimal as discussed previously); and (ii) a cylindrical shearing mechanism between helices (due to the close inter-plate spacing) with capacity $Q_{cs}$ estimated from Eq. 14 to 16 as per Mitsch and Clemence (1985):

$$Q_{cs,i} = \sigma_{v,i} K_{u,i} tan\varphi_{pi} \pi D_{h\_ave,i} \quad 14$$

$$K_{u,i} = 0.6 + m\frac{H_{ave,i}}{D_{h\_ave,i}} \quad 15$$

$$Q_{cs} = \sum_{i=1}^{n} Q_{cs,i} \quad 16$$

where $\sigma_{v,i}$ is the average in-situ vertical soil stress, $D_{h\_ave,i}$ is the average diameter of shearing cylinders, $H_{ave,i}$ is the average depth of shearing cylinders, and $K_{u,i}$ is a passive lateral earth pressure coefficient for the shearing cylinders which is a function of an empirical factor, $m$, estimated from Table 6.

Table 7 shows the predictions using Eq. 14 to 16. It is notable that the PM test results are over predicted by the approach and self-weight installation is under predicted highlighting the soil disturbance induced by pitch-matched installation and the potential of soil enhancement above helices by self-weight installation. It is also noteworthy that this approach appears to work well for challenging DOL case apparently supporting the assumption of interaction between lower and mid-height helices as proposed in Figure 4b, and further demonstrating the benefit of closer (more) helices in homogenising the capacity that can be achieved across a range of contrasting soil conditions by forcing a cylindrical shear mechanism in each case.

### *4.3 Performance of the tensile capacity prediction techniques*

The process undertaken above highlights that accounting for both helix geometry and soil layering is challenging for existing calculation approaches where detailed information on the various controlling mechanisms over the pile length are unknown or assumed. The 'Modified Giampa Method' performed well for 2H piles across the experimental dataset, although the DOL required empirical assumptions which would require further investigation for other similar strong-over weak soil cases to generalise. Therefore, it may be advantageous in practical design in such cases to conduct some initial simple wished-in-place numerical modelling (e.g. finite element analysis or limit analysis) to inform mechanistic behaviour. The Mitch and Clemence (1985) approach appeared to work well for 3H piles across all layering cases and installation methods, mainly as it forces a cylindrical shear mechanism independent of the soil layering and because the middle helix causes disturbance which homogenises the soil state. Therefore, more closely space (more) helices can result in good prediction of capacity that is more likely to be achieved if unexpected variability in ground conditions are encountered during installation. Ultimately though for confidence in pile capacity predictions under complex ground conditions large deformation numerical modelling (e.g. DEM) or centrifuge testing may be required to verify design.

## 5 Conclusion

A series of centrifuge tests were conducted to investigate installation and tensile performance of screw piles in uniform and layered sands. The piles were installed by either conventional displacement-controlled (pitch-matched, PM) or novel force-controlled (pile self-weight, SW) approaches prior to tensile loading tests, where the effect of SW installation on tensile response in sand had not previously been verified physically. The key findings are as follows:

When a widely spaced helix is located in a loose layer with overlying dense soil (DOL), the failure mechanism may be contained within the lower loose layer and overall pile tensile capacity can be improved by adding another helix near to the overlying dense layer to mobilise greater capacity. For a bottom helix in a dense layer a shallow truncated cone failure mechanism can develop to the surface. In this case an additional helix wound not improve capacity and may even result in a reduction of peak capacity from soil disturbance in dense soil layers due to the passage of the additional helix. For multi-helix piles with closer helix spacing, a cylindrical shear mechanism is forced, irrespective of the soil layering, and this, combined with homogenisation of soil properties due to soil disturbance in the denser material, results in a pile/anchor with an uplift capacity which is far less sensitive to the ground conditions. This has the potential to enable standardisation of pile designs across a variable site, or reduce the risk associated with encountering unexpected soil conditions during installation.

Self-weight installation can remove the need for additional vertical or crowd force and reduce torque during installation, reducing requirements on installation plant. This approach was also found to increase tensile capacity for a specific pile design consistent with over-flighted installation findings reported in previous research. Conducting self-weight installation in loose sand resulted in higher AR values because less penetration resistance at the pile base and shaft needs to be overcome by tensile force created by the over-flighted helix. Increasing helix number can also lead to increased AR values for self-weight installation due to additional helices providing extra tensile force to pull the pile into ground.

For screw piles with large helix-spacings (or a single helix at the bottom) where an individual bearing mechanism is expected for each helix, the Giampa *et al.* (2017) method, as modified in this study for layered soil conditions, gives reasonable predictions across the range of ground conditions considered. For piles with multiple helices (reduced helix spacing), the existing Mitsch and Clemence (1985) method appears appropriate for layered sands.

## 6 Acknowledgement

This study was funded by the Scheme for Promotion of Academic and Research (SPARC) to allow collaboration between Indian Researchers and other international centres of research and teaching excellence. The second author acknowledges financial support from China Scholarship Council and University of Dundee. The Fifth author was funded by the EPSRC NPIF funded studentship with Roger Bullivant Limited (Grant no. 617 EP/R512473/1).

## 7 Notation List

The following symbols are used in this paper:

| | | |
|---|---|---|
| 399 | $AR$ | advancement ratio |
| 400 | $B_i$ | diameter of a failure mechanism cone (Figure 14) |
| 401 | $D_{h,b}$ | diameter of the bottom helix |
| 402 | $D_{h,m}$ | diameter of the middle helix |
| 403 | $D_{h,t}$ | diameter of the top helix |
| 404 | $D_h$ | helix or anchor plate diameter |
| 405 | $D_{h\_ave}$ | average helix diameter for cylindrical shearing mechanism |
| 406 | $D_r$ | soil relative density |
| 407 | $D_s$ | pile shaft diameter |
| 408 | $d_z$ | pile uplift displacement |
| 409 | $F_b$ | installation vertical force on pile base |
| 410 | $F_h$ | installation vertical force on helix |
| 411 | $F_{h,u}$ | installation vertical force on helix |
| 412 | $F_{h,l}$ | installation vertical force on helix |
| 413 | $H$ | helix or anchor plate embedment depth |
| 414 | $H_i$ | height of a failure mechanism cone (Figure 14) |
| 415 | $H_{ave}$ | average depth for cylindrical shearing mechanism |
| 416 | $H_b$ | embedment depth of the bottom helix |
| 417 | $H_m$ | embedment depth of the middle helix |
| 418 | $H_t$ | embedment depth of the top helix |
| 419 | $K_u$ | passive lateral earth pressure coefficient |
| 420 | $l$ | height of a failure mechanism cone |
| 421 | $LB$ | layer boundary |
| 422 | $N_r$ | break-out factor for a helical plate or plate anchor |
| 423 | $PM$ | pitch-matched |
| 424 | $p_h$ | helix geometric pitch |
| 425 | $Q_{t,gia}$ | predicted tensile capacity of using Giampa et al. (2017) method |
| 426 | $Q_{t,gia,ht}$ | top helix component of predicted tensile capacity of using Giampa et al. (2017) method |
| 427 | $Q_{t,pm}$ | measured tensile capacity of a screw pile installed at AR = 1.0 |

| | | |
|---|---|---|
| 428 | $Q_{t,sw}$ | measured tensile capacity of a screw pile installed under self-weight conditions |
| 429 | $Q_t$ | tensile capacity of a screw pile |
| 430 | $SW$ | self-weight |
| 431 | $z$ | pile installation depth |
| 432 | $\sigma_v'$ | vertical component of soil effective stress |
| 433 | $\varphi_p$ | soil peak friction angle |
| 434 | $\psi_p$ | soil peak dilation angle |

435

436 **8 References**


437 Al-Baghdadi, T. (2018). Screw piles as offshore foundations: Numerical and physical modelling. Ph.D Thesis, University
438 of Dundee, UK.
439 Al-Baghdadi, T., Brown, M. J., Knappett, J. A., and Ishikura, R. (2015). Modelling of laterally loaded screw piles with
440 large helical plates in sand. In *Proceedings of 3rd International Symposium on Frontiers in Offshore Geotechnics,*
441 *ISFOG 2015* (M. Vaughan (ed)), Oslo, Norway, 10-12, June, pp. 503-508. CRC Press.
442 Al-Defae, A. H., Caucis, K., and Knappett, J. A. (2013). Aftershocks and the whole-life seismic performance of granular
443 slopes. *Geotechnique*, **63**, No. 14, 1230-1244.
444 Al Hakeem, N., and Aubeny, C. (2019). Numerical Investigation of Uplift Behavior of Circular Plate Anchors in Uniform
445 Sand. *Journal of Geotechnical and Geoenvironmental Engineering*, **145**, No. 9.
446 Bhattacharya, P., and Kumar, J. (2016). Uplift Capacity of Anchors in Layered Sand Using Finite-Element Limit Analysis:
447 Formulation and Results. *International Journal of Geomechanics*, **16**, No. 3.
448 Bittar, E., Lehane, B. M., Blake, A., Richards, D., White, D., Mahdavi, S., and Cerfontaine, B. (2024). CPT-based design
449 method for helical piles in sand. *Canadian Geotechnical Journal*, **61**, No. 1, 102-117.
450 Bolton, M. D., Gui, M. W., Garnier, J., Corte, J. F., Bagge, G., Laue, J., and Renzi, R. (1999). Centrifuge cone penetration
451 tests in sand. *Geotechnique*, **49**, No. 4, 543-552.
452 Bouazza, A., and Finlay, T. W. (1990). Uplift capacity of plate anchors buried in a two-layered sand. *Geotechnique*, **40**,
453 No. 2, 293-297.
454 Bradshaw, A., Zuelke, R., Hilderbranndt, L., Robertson, T., and Mandujano, R. (2019). Physical modelling of a helical pile
455 installed in sand under constant crowd. In *Proceedings of 1st International Symposium on Screw Piles for Energy*
456 *Applications* (C. Davidson, M. J. Brown, J. Knappett, and A. J. Brennan (eds)), Dundee, UK, 27-28 May, 2019, pp.
457 109-115. University of Dundee, Dundee, UK.
458 British Standards Institution (2015). BS8004: Code of practice for foundations. BSI, London, UK.
459 Cerato, A. B., and Victor, R. (2009). Effects of long-term dynamic loading and fluctuating water table on helical anchor
460 performance for small wind tower foundations. *Journal of Performance of Constructed Facilities*, **23**, No. 4, 251-261.
461 Cerfontaine, B., Brown, M. J., Knappett, J. A., Davidson, C., Sharif, Y. U., Huisman, M., Ottolini, M., and Ball, J. D.
462 (2023a). Control of screw pile installation to optimise performance for offshore energy applications. *Géotechnique*, **73**,
463 No. 3, 234-249.
464 Cerfontaine, B., Ciantia, M. O., Brown, M. J., and Sharif, Y. U. (2021). DEM study of particle scale and penetration rate
465 on the installation mechanisms of screw piles in sand. *Computers and Geotechnics*, **139**.
466 Cerfontaine, B., White, D., Kwa, K., Gourvenec, S., Knappett, J., and Brown, M. (2023b). Anchor geotechnics for floating
467 offshore wind: Current technologies and future innovations. *Ocean Engineering*, **279**.
468 Das, B., and Shukla, S. K. (2013). *Earth Anchors*, J. Ross Publishing, Florida, USA.
469 Davidson, C., Al-Baghdadi, T., Brown, M. J., Knappett, J., Brennan, A. J., and Augarde, C. E. (2018). Centrifuge modelling
470 of screw piles for offshore wind energy foundations. In *Proceedings of Physical Modelling in Geotechnics: Proceedings*
471 *of the 9th International Conference on Physical Modelling in Geotechnics* (S. Mcnamara, S. Divall, and R. Goodey
472 (eds)), London, United Kingdom, pp. 695-700. Taylor & Francis.
473 Davidson, C., Brown, M., Cerfontaine, B., Al-Baghdadi, T., Knappett, J., Brennan, A. J., Augarde, C., Coombs, W. M.,
474 Wang, L., Blake, A., Richards, D., and Ball, J. (2022). Physical modelling to demonstrate the feasibility of screw piles
475 for offshore jacket-supported wind energy structures. *Geotechnique*, **72**, No. 2, 108-126.

Feng, S. J., Fu, W. D., Chen, H. X., Li, H. X., Xie, Y. L., Lv, S. F., and Li, J. (2020). Field tests of micro screw anchor piles under different loading conditions at three soil sites. *Bulletin of Engineering Geology and the Environment*, **80**, No. 1, 127-144.

Ghaly, A., Hanna, A., and Hanna, M. (1991). Uplift Behavior of Screw Anchors in Sand. I: Dry Sand. *Journal of Geotechnical Engineering-ASCE*, **117**, No. 5, 773-793.

Giampa, J. R., Bradshaw, A. S., and Schneider, J. A. (2017). Influence of Dilation Angle on Drained Shallow Circular Anchor Uplift Capacity. *International Journal of Geomechanics*, **17**, No. 2.

Knappett, J., Brown, M., Brennan, A., and Hamilton, L. (2014). Optimising the compressive behaviour of screw piles in sand for marine renewable energy applications. In *Proceedings of Conference On Piling & Deep Foundations*, Stockholm, Sweden.

Kumar, P. V. P., Patra, S., Haldar, S., Brown, M. J., Knappett, J. A., and Sharif, Y. U. (2023). 3D numerical analysis of screw pile subjected to axial compressive and lateral load. In *Proceedings of Soil Dynamics, Earthquake and Computational Geotechnical Engineering. IGC 2021* (K. Muthukkumaran, R. Ayothiraman, and S. Kolathayar (eds)) vol. 5. Springer Nature.

Lauder, K. (2010). The performance of pipeline ploughs. Ph.D Thesis, University of Dundee, UK.

Li, W., Deng, L., and Chalaturnyk, R. (2022). Centrifuge modeling of the behaviour of helical piles in cohesive soils from installation and axial loading. *Soils and Foundations*, **62**, No. 3.

Lutenegger, A. J. (2011). Behavior of Multi-Helix Screw Anchors in Sand. In *Proceedings of 14th Pan-American Conference on Soil Mechanics and Geotechnical Engineering*, Toronto, Ontario, Canada, October 2-6. Canadian Geotechnical Society.

Meyerhof, G. G., and Adams, J. I. (1968). The Ultimate Uplift Capacity of Foundations. *Canadian Geotechnical Journal*, **5**, No. 4.

Mitsch, M. P., and Clemence, S. P. (1985). The uplift capacity of helix anchors in sand. In *Proceedings of Uplift Behavior of Anchor Foundations in Soil*, New York, USA. American Society of Civil Engineers.

Perko, H. (2009). *Helical Piles A Practical Guide to Design and Installation*, John Wiley & Sons, New Jersey, US.

Saeedy, H. S. (1987). Stability of circular vertical earth anchors. *Canadian Geotechnical Journal*, **24**, No. 3, 452-456.

Sakai, T., and Tanaka, T. (2007). Experimental and numerical study of uplift behavior of shallow circular anchor in two-layered sand. *Journal of Geotechnical and Geoenvironmental Engineering*, **133**, No. 4, 469-477.

Schiavon, A. J. (2016). Behaviour of helical anchors subjected to cyclic loadings.Ph.D Thesis, Universidade de São Paulo, Brazil.

Schiavon, J. A., Tsuha, C. H. C., and Thorel, L. (2017). Cyclic and post-cyclic monotonic response of a single-helix anchor in sand. *Géotechnique Letters*, **7**, No. 1, 11-17.

Sharif, Y. U. (2024). The effects of rotary installation on the axial capacity of displacement piles in sand. Ph.D, University of Dundee, Dundee, UK.

Sharif, Y. U., Brown, M. J., Cerfontaine, B., Davidson, C., Ciantia, M. O., Knappett, J. A., Ball, J. D., Brennan, A., Augarde, C., Coombs, W., Blake, A., Richards, D., White, D., Huisman, M., and Ottolini, M. (2021a). Effects of screw pile installation on installation requirements and in-service performance using the discrete element method. *Canadian Geotechnical Journal*, **58**, No. 9, 1334-1350.

Sharif, Y. U., Brown, M. J., Ciantia, M. O., Cerfontaine, B., Davidson, C., Knappett, J. A., and Ball, J. (2021b). Assessing single-helix screw pile geometry on offshore installation and axial capacity. *Proceedings of the Institution of Civil Engineers - Geotechnical Engineering*, **174**, No. 5, 512-529.

Spagnoli, G., and Tsuha, C. (2020). A review on the behavior of helical piles as a potential offshore foundation system. *Marine Georesources & Geotechnology*, **38**, No. 9, 1013-1036.

Srinivasan, V., Ghosh, P., and Santhoshkumar, G. (2019). Experimental and Numerical Analysis of Interacting Circular Plate Anchors Embedded in Homogeneous and Layered Cohesionless Soil. *International Journal of Civil Engineering*, **18**, No. 2, 231-244.

Stewart, W. (1985). Uplift capacity of circular plate anchors in layered soil. *Canadian Geotechnical Journal*, **22**, No. 4, 589-592.

Tsuha, C. H. C., Aoki, N., Rault, G., Thorel, L., and Garnier, J. (2012). Evaluation of the efficiencies of helical anchor plates in sand by centrifuge model tests. *Canadian Geotechnical Journal*, **49**, No. 9, 1102-1114.

Ullah, S. N., O'Loughlin, C., Hu, Y., and Hou, L. F. (2023). Torsional installation and vertical tensile capacity of helical piles in clay. *Géotechnique*, 1-17.

Wang, W., Brown, M. J., Sharif, Y. U., and Davidson, C. (2023). The influence of the installation advancement ratio on the cyclic performance of a single-helix pile for floating offshore wind applications. In *Proceedings of 9th International SUT OSIG Conference - Innovative Geotechnologies for Energy Transition*, London, UK, September, 12-14, pp. 1218-1224. Society for Underwater Technology.

Wang, W., Brown, M. J., Sharif, Y. U., Davidson, C., and Ciantia, M. O. (2025a). Centrifuge Modeling of the Installation Advancement Ratio Effect on the Cyclic Response of a Single-Helix Screw Pile for Floating Offshore Wind. *Journal of Geotechnical and Geoenvironmental Engineering*, **151**, No. 1.

Wang, W., John Brown, M., Oryem Ciantia, M., Previtali, M., Umar Sharif, Y., and Davidson, C. (2025b). The effect of installation advancement ratio on interaction between helices of screw piles for offshore renewable energy. *Ocean Engineering*, **316**.
Yang, J. (2006). Influence zone for end bearing of piles in sand. *Journal of Geotechnical and Geoenvironmental Engineering*, **132**, No. 9, 1229-1237.

## 9 Table list

*Table 1 Properties of the HST95 sand (Al-Defae et al. 2013; Lauder 2010)*

| Properties | Symbol | Value | Dense (D) | Loose (L) |
|---|---|---|---|---|
| Effective particle size [mm] | $d_{10}$ | 0.090 | - | - |
| Mean particle size [mm] | $d_{50}$ | 0.141 | - | - |
| Particle specific gravity [-] | $G_s$ | 2.63 | - | - |
| Minimum void ratio [-] | $e_{min}$ | 0.467 | - | - |
| Maximum void ratio [-] | $e_{max}$ | 0.769 | - | - |
| Relative density | $D_r$ | - | 75% | 30% |
| Dry unit weight [kN/m$^3$] | $\gamma_{dry}$ | 14.5+3×$D_r$ | 16.8 | 15.4 |
| Saturated unit weight [kN/m$^3$] | $\gamma_{sat}$ | 18.8+1.8×$D_r$ | 20.1 | 19.3 |
| Critical state friction angle [°] | $\varphi_{cs}$ | 32 | - | - |
| Peak friction angle [°]* | $\varphi_p$ | 29+20×$D_r$ | 44.0 | 35.0 |
| Peak dilation angle [°]* | $\psi_p$ | -4.4+26×$D_r$ | 15.1 | 3.4 |
| Steel-sand interface friction angle [°] | $\delta$ | 24 | - | - |

* Determined for confining effective stresses of 20 kPa - 500 kPa

546 *Table 2 Summary of tests conducted and key results (shown at prototype scale)*

| Test ID | Pile ID | Soil bed profile ID | Installation mode | Final installation compressive force (kN) | Final installation torque (kNm) | Tensile capacity (kN) | Disp. at peak loading (m) |
|---|---|---|---|---|---|---|---|
| 2H_UD_AR1 | 2H | UD ($D_r$ = 75%) | AR = 1.0 | 1839.8 | 382.3 | 1236.1 | 0.077 |
| 3H_UD_AR1 | 3H | UD ($D_r$ = 75%) | AR = 1.0 | 1529.0 | 277.2 | 839.9 | 0.071 |
| 2H_DOL_AR1 | 2H | DOL ($D_r$ = 75% over 30%) | AR = 1.0 | 446.7 | 85.0 | 203.7 | 0.070 |
| 3H_DOL_AR1 | 3H | DOL ($D_r$ = 75% over 30%) | AR = 1.0 | 921.0 | 279.6 | 595.7 | 0.074 |
| 2H_LOD_AR1 | 2H | LOD ($D_r$ = 30% over 75%) | AR = 1.0 | 823.0 | 154.9 | 678.9 | 0.092 |
| 3H_LOD_AR1 | 3H | LOD ($D_r$ = 30% over 75%) | AR = 1.0 | 1624.0 | 363.7 | 717.3 | 0.092 |
| 2H_DLD_AR1 | 2H | DLD ($D_r$ = 75% -30% -75%) | AR = 1.0 | 1243.0 | 228.4 | 944.9 | 0.102 |
| 3H_DLD_AR1 | 3H | DLD ($D_r$ = 75% -30% -75%) | AR = 1.0 | 1880.7 | 442.2 | 835.0 | 0.090 |
| 2H_DOL_SW | 2H | DOL ($D_r$ = 75% over 30%) | SW | - | 65.5 | 463.9 | 0.057 |
| 3H_DOL_SW | 3H | DOL ($D_r$ = 75% over 30%) | SW | - | 204.4 | 729.9 | 0.040 |
| 2H_LOD_SW | 2H | LOD ($D_r$ = 30% over 75%) | SW | - | 183.7 | 956.6 | 0.040 |
| 3H_LOD_SW | 3H | LOD ($D_r$ = 30% over 75%) | SW | - | 251.4 | 933.6 | 0.046 |
| 3H_DOL_AR035 | 3H | DOL ($D_r$ = 75% over 30%) | AR = 0.35 | -422.5 | 183.3 | 831.7 | 0.033 |

547

548

549 *Table 3 Tensile capacity predictions using proposed modified Giampa et al. (2017) model (Eq. 2-9) compared to centrifuge testsg for*

550 *2H pile in uniform and layered soil ($l_1$ = 2.5 m and $l_2$ = 3.0 m adopted for DOL although the failure is assumed as deep)*

| | | Predicted | | Measured | | Predicted/ Measured | |
|---|---|---|---|---|---|---|---|
| Soil profile | Assumed failure mode | Top helix $Q_{t,gia,ht}$ (kN) | Total $Q_{t,gia}$ (kN) | Pitch-matched $Q_{t,pm}$ (kN) | Self-weight $Q_{t,sw}$ (kN) | $Q_{t,gia}/Q_{t,pm}$ | $Q_{t,gia}/Q_{t,sw}$ |
| UD | Shallow | 9.2 | 1317.8 | 1236.1 | - | 1.07 | - |
| DOL | Deep | 9.2 | 776.6 | 203.7 | 463.9 | 3.81 | 1.67 |
| LOD | Shallow | 7.7 | 867.1 | 678.9 | 956.6 | 1.28 | 0.91 |
| DLD | Shallow | 9.2 | 1028.1 | 944.9 | - | 1.09 | - |

551

*Table 4 Calculated deep tensile capacity for 2H in DOL using Eq.10 ($Q_{t,pm}$ and $Q_{t,sw}$ are measured capacity at AR = 1.0 and self-weight installation conditions)*

| Reference | Anchor type | Modelling approach | $N_r$ | Calculated capacity, (kN) | Measured $Q_{t,pm}$ (kN) | Measured $Q_{t,sw}$ (kN) | Predicted/Measured Predicted $/Q_{t,pm}$ | Predicted/Measured Predicted $/Q_{t,sw}$ |
|---|---|---|---|---|---|---|---|---|
| Meyerhof and Adams (1968) | Plate anchor | 1g | 18 | 456.0 | 203.7 | 463.9 | 2.24 | 0.98 |
| Saeedy (1987) | Plate anchor | 1g | 29 | 733.0 | | | 3.60 | 1.58 |
| Mitsch and Clemence (1985) | Screw pile | 1g | 52 | 1314.4 | | | 6.45 | 2.83 |
| Al Hakeem and Aubeny (2019) | Plate anchor | FE | 21 | 530.8 | | | 2.60 | 1.14 |
| This study (AR = 1.0) | Screw pile | Centrifuge | 8 | - | - | - | - | - |
| This study (self-weight) | Screw pile | Centrifuge | 18 | - | - | - | - | - |

*Table 5 Tensile capacity for 2H pile predicted using UWASP-22 CPT approach (total capacity $Q_{t,uwa}$, subscript h,b = bottom helix, s = shaft) compared to centrifuge results*

| Soil profile | Pile ID | Predicted | | | Measured | | Predicted/Measured | |
|---|---|---|---|---|---|---|---|---|
| | | $Q_{h,b,uwa}$ (kN) | $Q_{s,uwa}$ (kN) | $Q_{t,uwa}$ (kN) | Pitch-matched $Q_{t,pm}$ (kN) | Self-weight $Q_{t,sw}$ (kN) | $Q_{t,uwa}/Q_{t,pm}$ | $Q_{t,uwa}/Q_{t,sw}$ |
| UD | 2H | 623.8 | 135.0 | 758.8 | 1236.1 | - | 0.61 | - |
| DOL | 2H | 221.4 | 82.8 | 304.2 | 203.7 | 463.9 | 1.49 | 0.66 |
| LOD | 2H | 613.5 | 92.8 | 706.3 | 678.9 | 956.6 | 1.04 | 0.74 |
| DLD | 2H | 619.2 | 107.2 | 726.4 | 994.9 | - | 0.73 | - |

559 *Table 6 Values of m varying with soil friction angles, as derived by Mitsch and Clemence (1985) and Das and Shukla (2013)*

| Peak friction angle, $\varphi_p'$ (°) | $m$ |
|---|---|
| 25 | 0.033 |
| 30 | 0.075 |
| 35 | 0.180 |
| 40 | 0.250 |
| 45 | 0.289 |

560

561

562 *Table 7 Tensile capacity predictions using semi- empirical models (Eq.14~16) (Mitsch and Clemence 1985) compared to centrifuge*

563 *testing measurments for 3H pile*

| | Predicted | Measured | | | |
|---|---|---|---|---|---|
| Soil profile | $Q_{cs}$ (kN) | Pitch-matched $Q_{t,pm}$ (kN) | $Q_{cs}/Q_{t,pm}$ | Self-weight $Q_{t,sw}$ (kN) | $Q_{cs}/Q_{t,sw}$ |
| UD | 966.9 | 839.9 | 1.15 | - | - |
| DOL | 639.0 | 602.3 | 1.06 | 729.9 | 0.88 |
| LOD | 866.9 | 712.7 | 1.22 | 933.6 | 0.93 |
| DLD | 903.1 | 835.0 | 1.08 | - | - |

564

## 10 Figure list

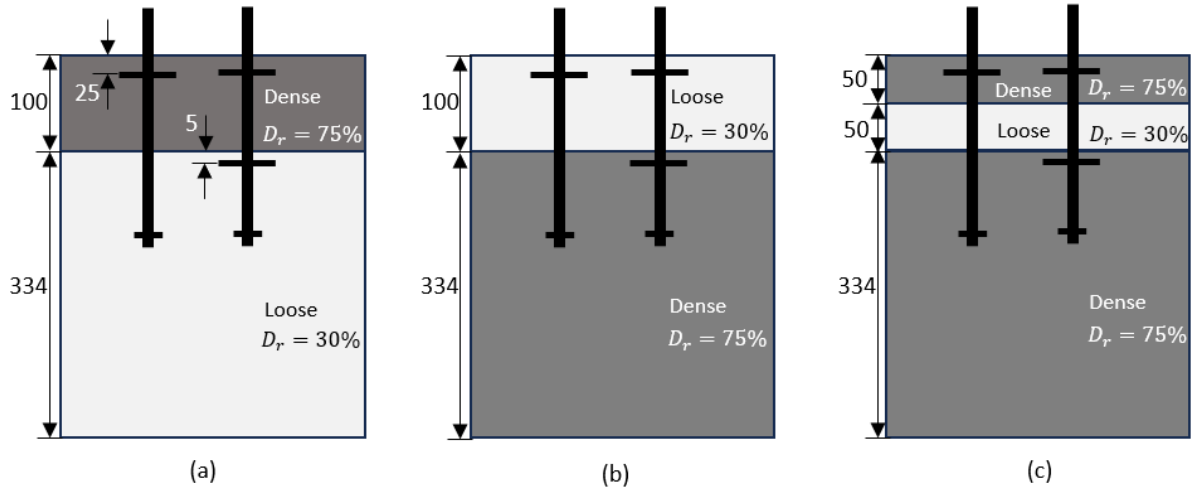


*Figure 1 Schematic plots of layered soil bed profiles with piles at final installation depth: (a) dense over loose (DOL), (b) loose over dense (LOD), (c) dense-loose-dense sandwich (DLD) (dimension unit: m at prototype scale, uniform dense layer not shown, not to scale)*

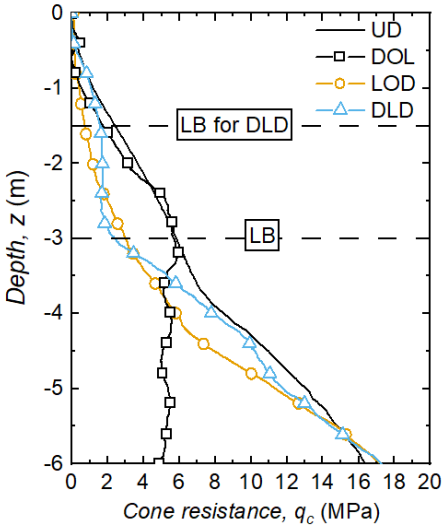


570

571 *Figure 2 Prototype CPT cone penetration resistance $q_c$ in soil beds studied (LB: layer boundary)*

572

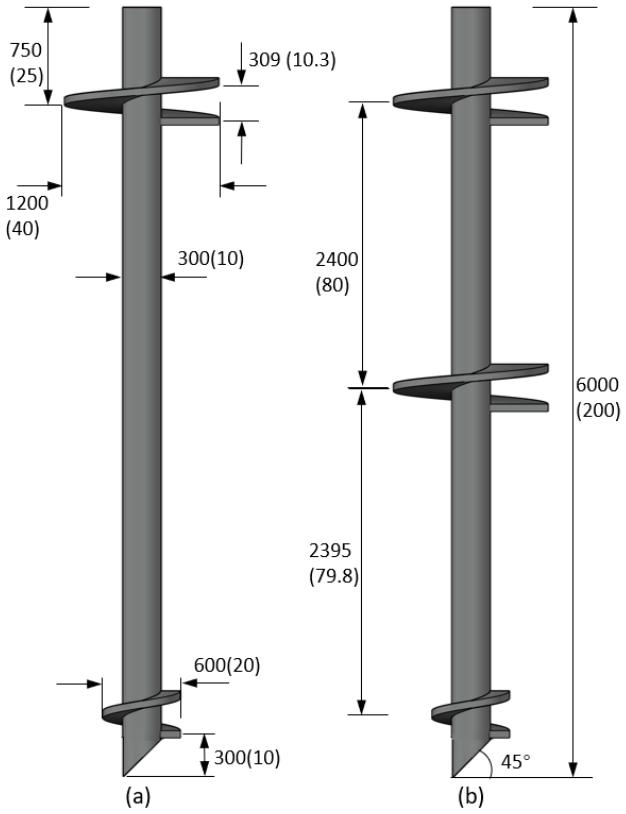


573

574 *Figure 3 Pile geometries studied shown at prototype scale in mm (a) 2H (b) 3H (model scale in brackets)*

575

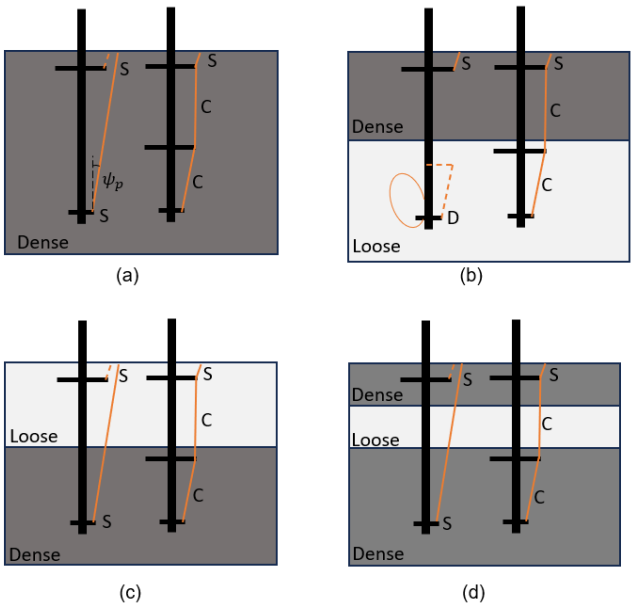


576

577 *Figure 4 Schematic illustration of screw pile assumed failure mechanisms in sand for the various layer combinations (a) uniform dense*

578 *(UD), (b) dense over loose (DOL), (c) loose over dense (LOD), (d) dense-loose-dense 'sandwich' (DLD) (D = deep, S = shallow, C =*

579 *cylindrical shearing)*

580

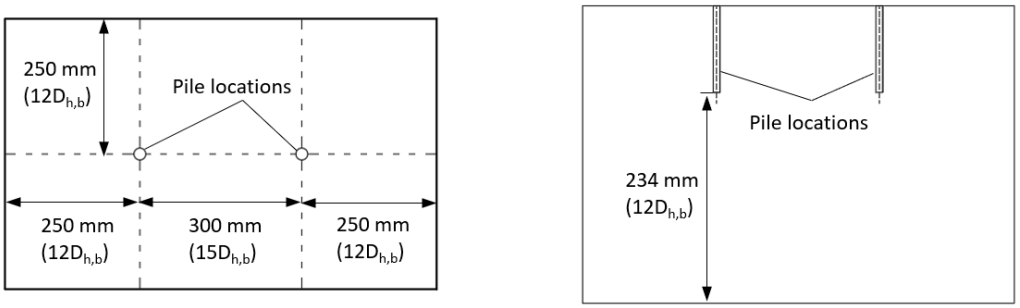


581

582 *Figure 5 (a) Plan and (b) front view of pile test locations in the strong box*

583

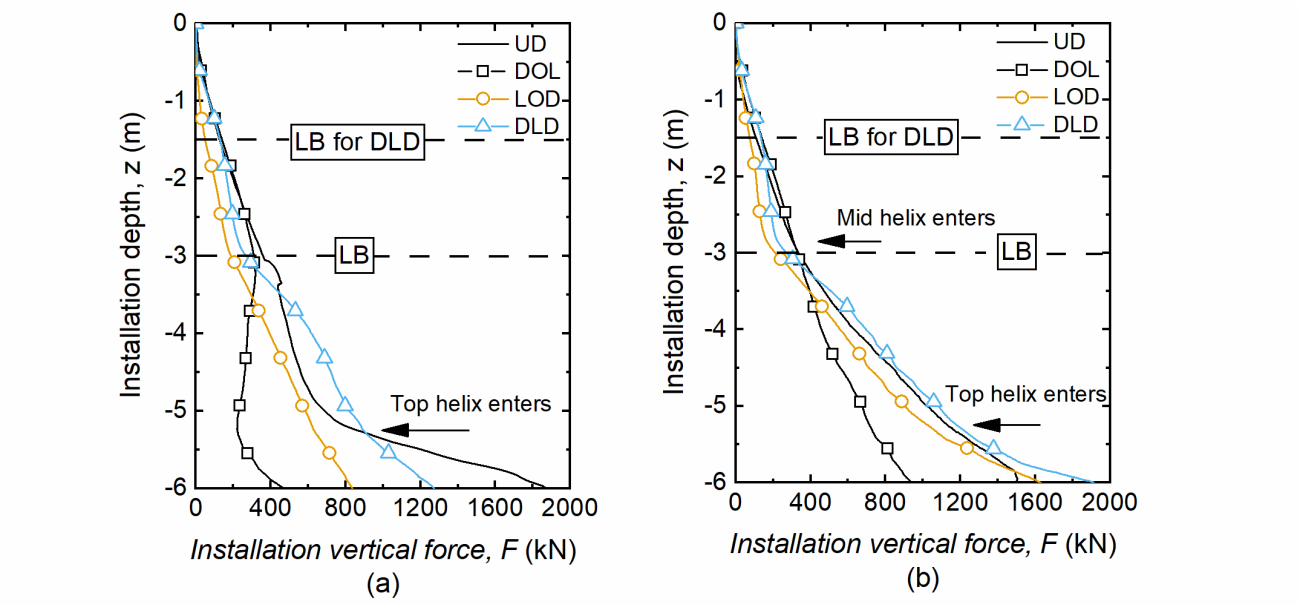


584

585 *Figure 6 Vertical force required for pitch matched (PM) installation (AR = 1.0) in different soil beds for (a) 2H pile and (b) 3H pile*

586 *(LB= layer boundary position, soil bed identification as per Figure 1 and Table 2)*

587

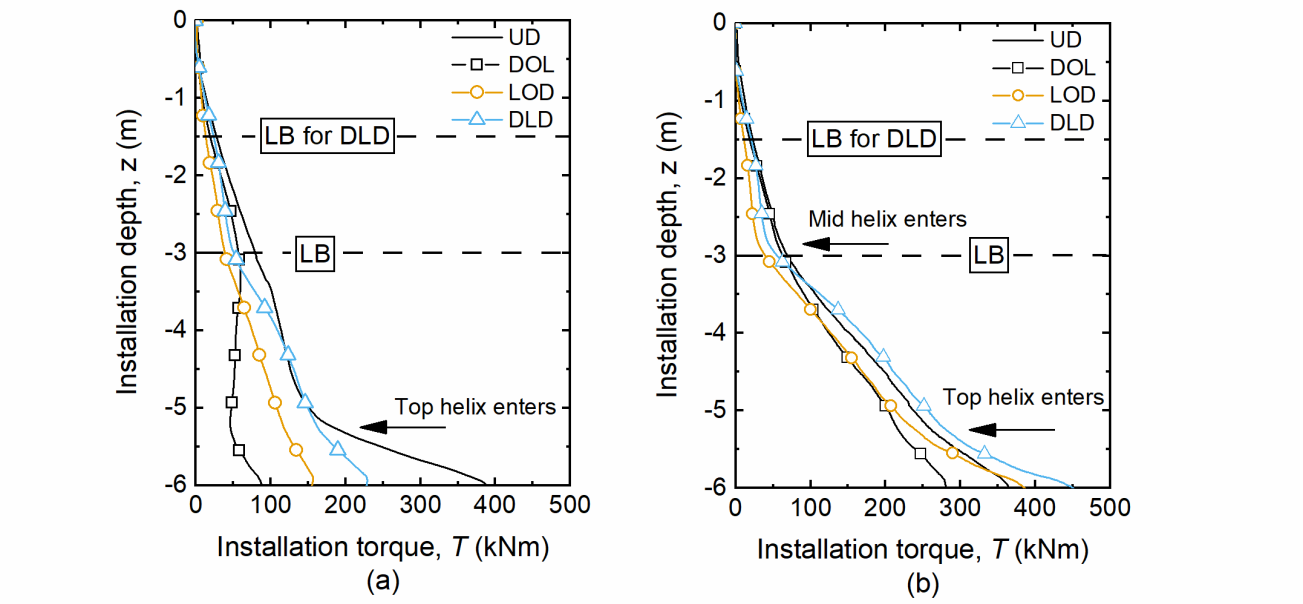


588

589 *Figure 7 Torque required for PM installation (AR = 1.0) in different soil beds for (a) pile 2H and (b) pile 3H (LB= layer boundary*

590 *position, soil bed identification as per Figure 1 and Table 2)*

591

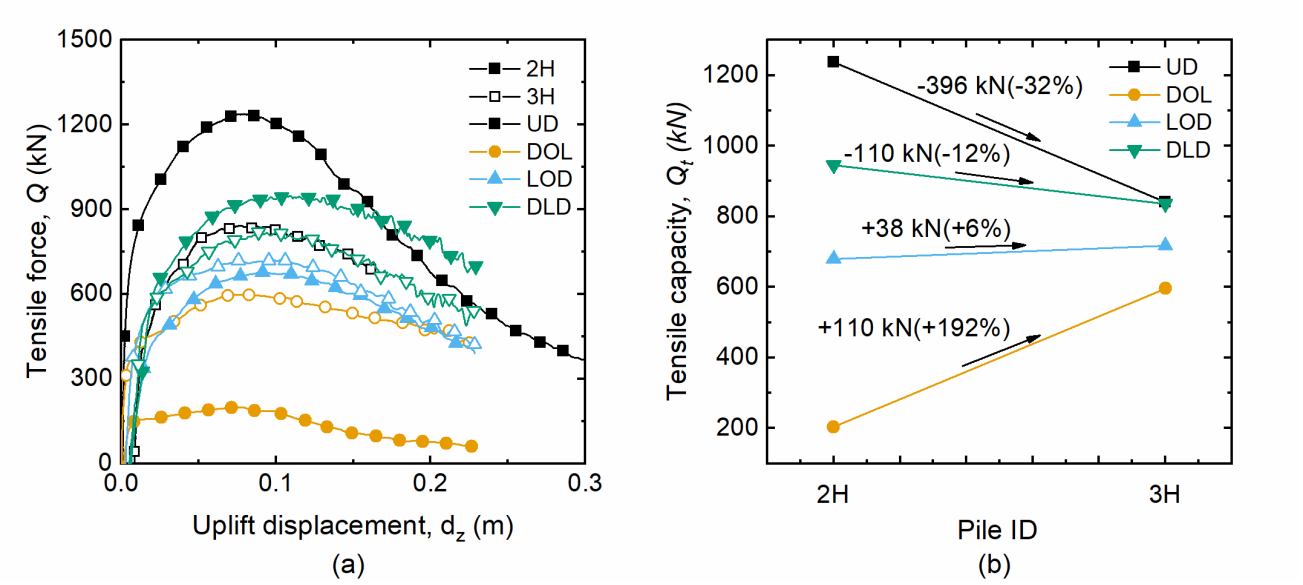


592

593 *Figure 8 Tensile response of 2H and 3H piles at AR = 1.0 (PM) in different soil layering regimes (a) load – displacement response (b)*

594 *effect of the mid helix inclusion on tensile capacity*

595

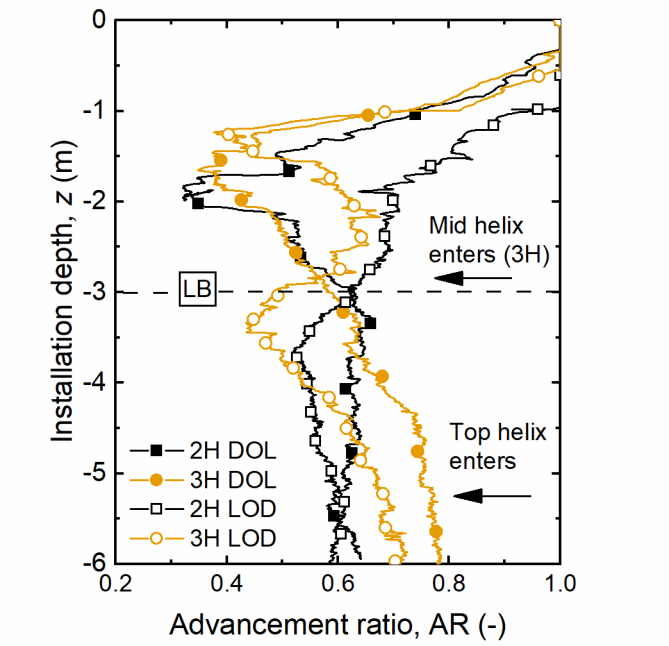


596

597 *Figure 9 Measured AR values during self-weight installation (LB: layer boundary)*

598

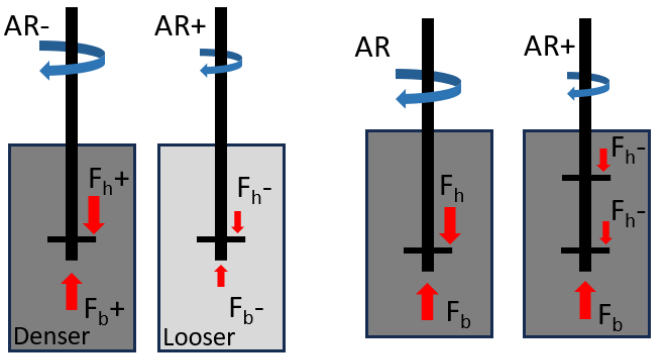


599

600 *Figure 10 Idealisation of effects of (a) soil relative density and (b) helix number on AR values during self-weight installation ($F_h$: vertical*

601 *force on helix, $F_b$: vertical force on pile end, + and – denote increase and decrease)*

602

603

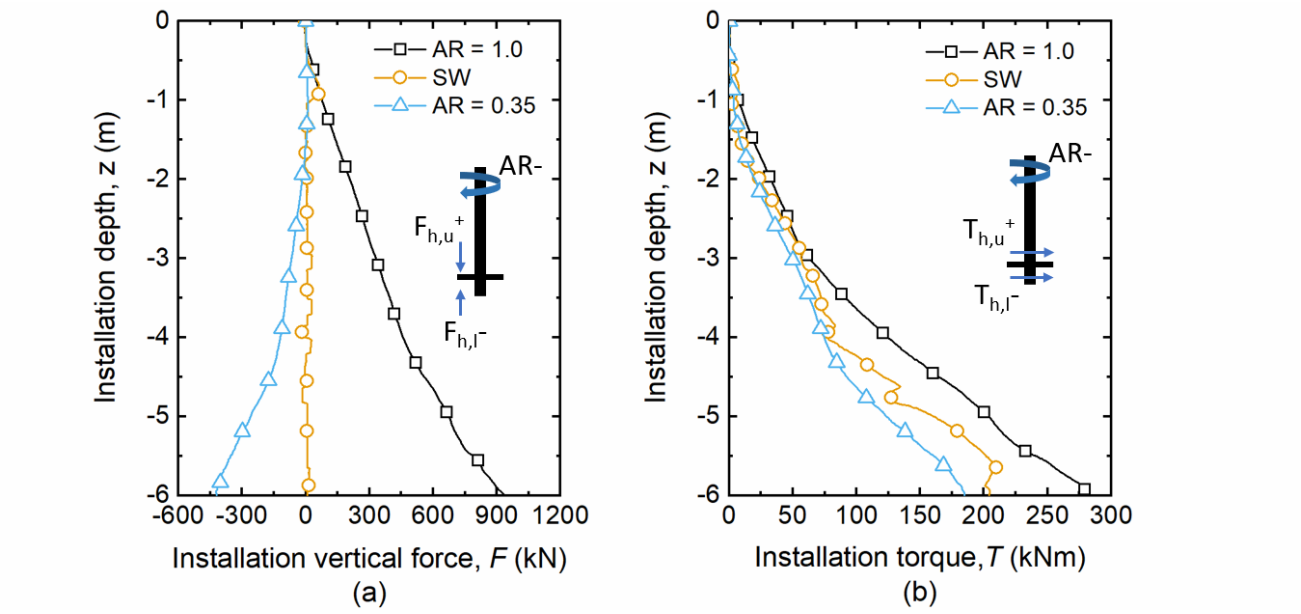


604

605 *Figure 11 Required (a) force and (b) torque for pile 3H in DOL soil bed during installation adopting different approaches (SW refers*
606 *to self-weight installation, $F_{h,u}$ and $F_{h,l}$: vertical force on upper and lower surface of helix, $T_{h,u}$ and $T_{h,l}$: torque on upper and lower*
607 *surface of helix, the sketch idealises behaviour of each single helix in the ground rather than the whole pile)*

608

609

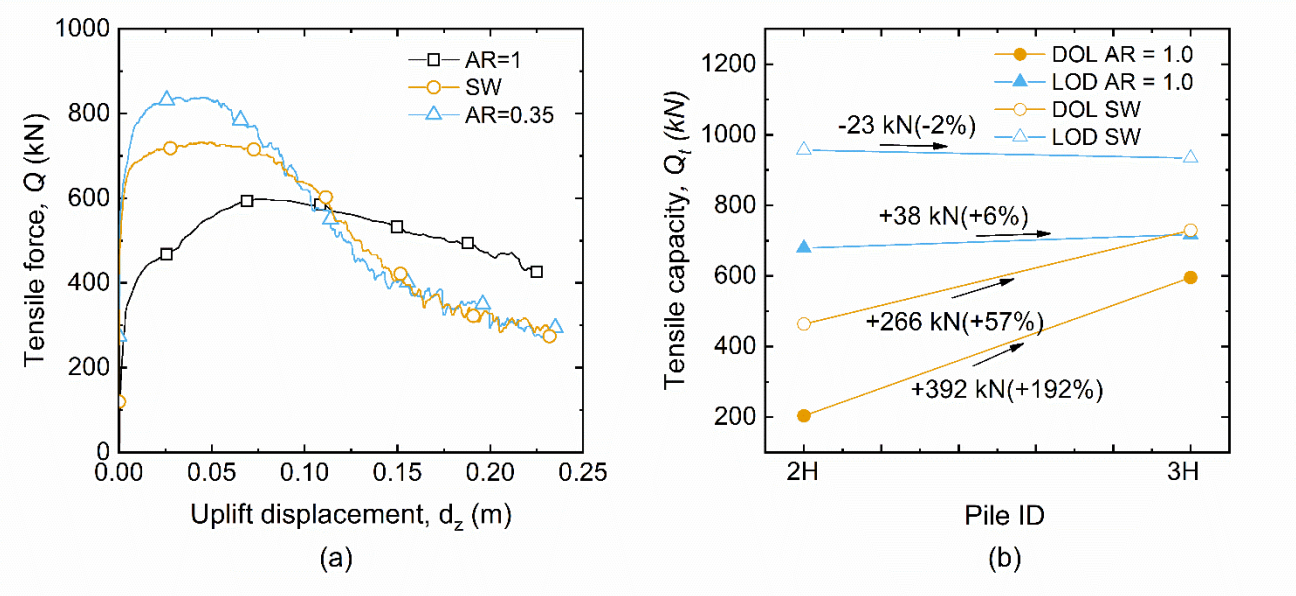


610

611 *Figure 12 (a) tensile force – displacement response of a 3H pile installed using different approaches in DOL soil bed (b) effect of helix*

612 *number, installation approach and soil bed profile on tensile capacity*

613

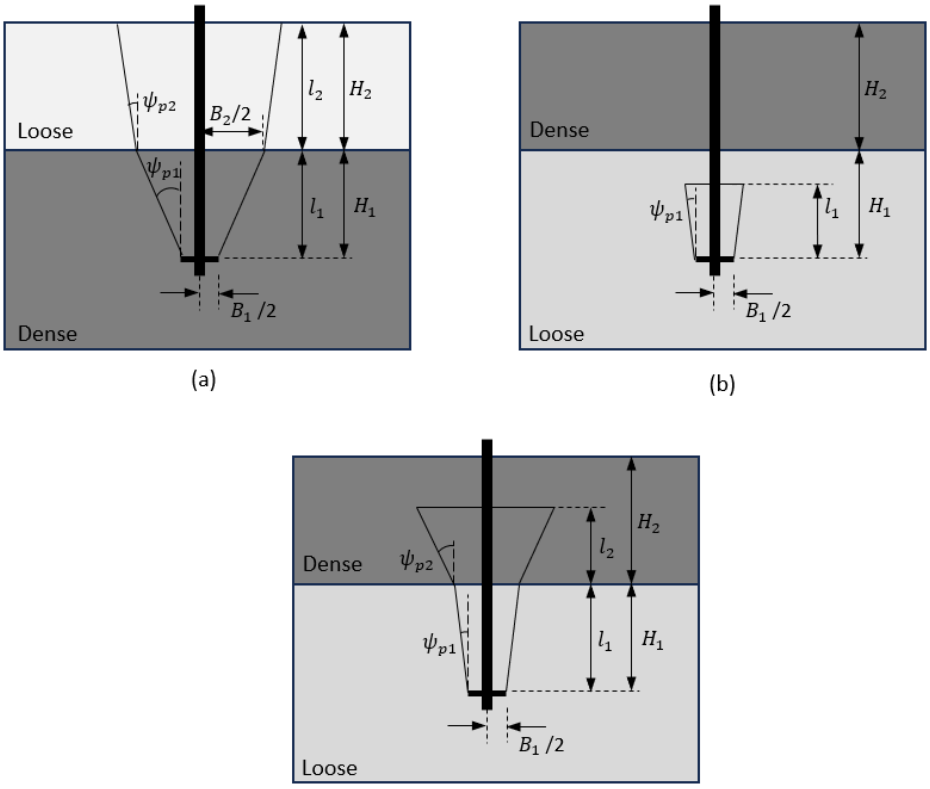


614

615 *Figure 13 Schematic explanation of failure mechanism inclined angle varying inclined angle at a layer boundary (a) loose over dense*
616 *layers (shallow) (b) dense over loose layers with failure mechanism being localised in the underlying layer (deep) (c) dense over loose*
617 *layers with failure mechanism developing to the overlying layer (deep)*

618

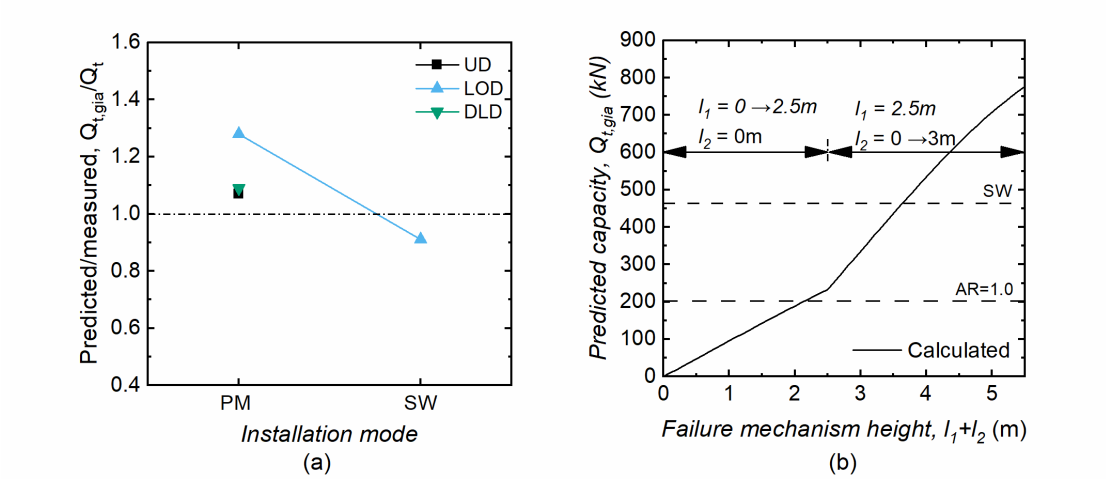


619

620 *Figure 14 Tensile capacity of 2H predicted using modified Giampa et al. (2017) method (Eq. 2-9) compared to the measured capacity*

621 *in centrifuge tests (a) shallow mechanism (UD, LOD and DLD) (b) deep mechanism (DOL)*

622

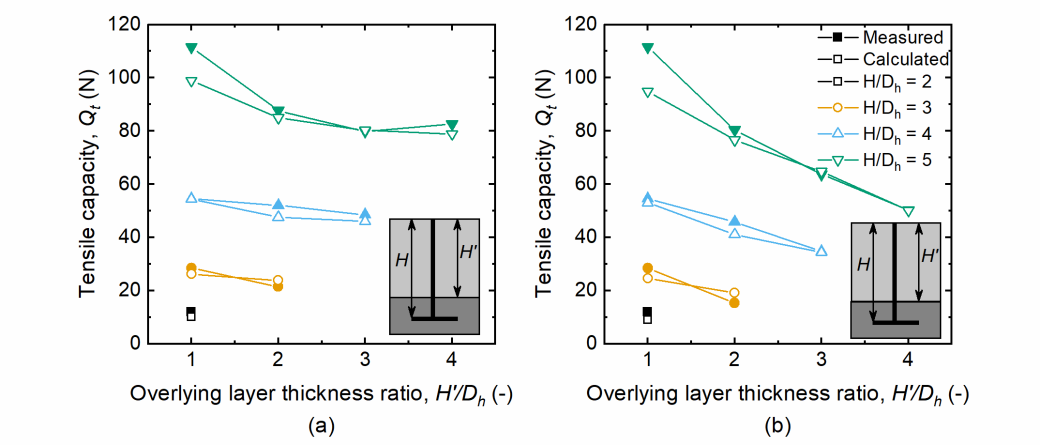


623

624 *Figure 15 Plate anchor tensile capacity in layered Leighton Buzzard sand, comparison between Bouazza and Finlay (1990) 1g tests*
625 *measurement and calculation from Eq. (2-9). Dense sand ($D_r$ = 89%) underlying (a) medium-dense ($D_r$ = 61%) and (b) loose sand ($D_r$*
626 *= 32%)*

627

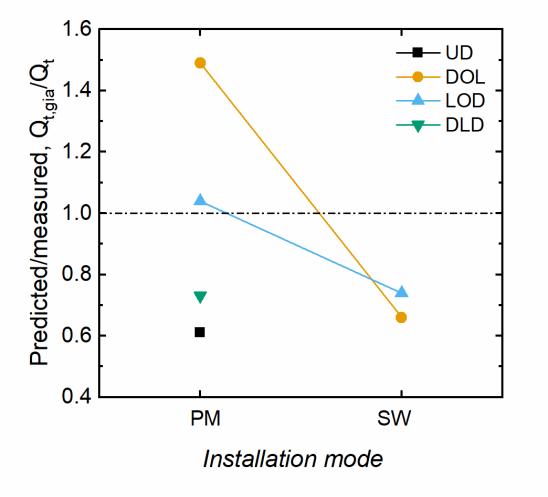


628

629 *Figure 16 Tensile capacity of 2H pile predicted using UWASP-22 (Bittar et al. 2024) compared to the measured capacity in centrifuge*

630 *tests*